
Article:
Wang, A., Fei, M., Li, X. et al. (2025) Plug-N-Play Voltage Control for DC Microgrids Feeding Constant Power Loads in More Electric Aircraft. IEEE Transactions on Aerospace and Electronic Systems, 62. 1211 -1224. ISSN: 0018-9251

https://doi.org/10.1109/taes.2025.3628333

Plug-n-Play Voltage Control for DC Microgrids Feeding Constant Power Loads in More Electric Aircraft

Aimin Wang, Graduate Student Member, IEEE
Minrui Fei
Xue Li, Member, IEEE
Chen Peng, Senior Member, IEEE
Shanghai University, Shanghai, China

Kang Li, Senior Member, IEEE
University of Leeds, Leeds, U.K

Chi Yung Chung, Fellow, IEEE
Hong Kong Polytechnic University, Hong Kong, China

***Abstract*— Aviation electrification has accelerated the adoption of onboard DC microgrids (DCMGs) in more electric aircraft (MEA). The dynamic integration and disconnection of renewable energy sources (RESs) are crucial for resource optimization and environmental adaptation but can induce voltage instability. This paper proposes a plug-n-play (PnP) voltage control strategy for MEAs operating under constant power loads (CPLs), ensuring voltage stability while enabling seamless RES connection and disconnection. A unified onboard DCMG model is formulated, capturing both the nonlinear behavior of CPLs and the interconnection couplings among RESs. Leveraging a structured storage function technique, sufficient conditions are derived to guarantee dissipative voltage stability at local and global levels. The proposed fully decentralized control scheme operates independently of both the number of RESs and their interconnection topology, thereby significantly enhancing the scalability for smooth plug-in/-out operations. Extensive simulations conducted across various scenarios convincingly validate the effectiveness of the proposed control strategy.**

***Index Terms*— More electric aircraft (MEA), DC microgrids (DCMGs), plug-n-play (PnP) voltage control, scalability, constant power load (CPL).**

This work was supported in part by the Natural Science Foundation of China (NSFC) under Grant U24A20259, 62173217, 62203290 and in part by the 111 Project under Grant D18003.

Authors' addresses: Aimin Wang, Minrui Fei, Xue Li, and Chen Peng are with the Shanghai Key Laboratory of Power Station Automation Technology, School of Mechatronic Engineering and Automation, Shanghai University, Shanghai 200072, China (e-mail: amwang@shu.edu.cn; mrfei@staff.shu.edu.cn; lixue@i.shu.edu.cn; c.peng@i.shu.edu.cn). Kang Li is with the School of Electronics and Electrical Engineering, University of Leeds, Leeds LS2 9JT, U.K. (e-mail: k.li1@leeds.ac.uk). Chi Yung Chung is with the Department of Electrical Engineering, The Hong Kong Polytechnic University, Hong Kong SAR 100872, China (e-mail: c.y.chung@polyu.edu.hk). *Corresponding authors: Minrui Fei and Xue Li.*

I. INTRODUCTION

With large commercial aircraft contributing over 75% of aviation emissions and air travel growing at 4%–5% annually, reducing the sector's environmental impact has become a critical priority [1]. To reduce aviation's carbon footprint, NASA introduced the N+3 aircraft concept, targeting a 75% reduction in landing/takeoff NO_x emissions and a 70% decrease in mission fuel consumption by 2035 [2]. Realizing these ambitious targets requires a shift toward electrified propulsion and power systems, positioning the more electric aircraft (MEA) paradigm as a pivotal solution [3]. By replacing traditional hydraulic, pneumatic, and mechanical systems with electrical alternatives, MEAs can significantly reduce fuel consumption, emissions, and maintenance complexity [4]–[6]. Among these advancements, onboard DC microgrids (DCMGs) have emerged as a promising power distribution architecture for MEAs, offering lower conversion losses, improved energy storage integration, and simplified control [7]. Unlike AC microgrids, DCMGs avoid frequency and reactive power regulation issues, facilitating the direct integration of battery energy storage systems (BESSs) and renewable energy sources (RESs), including fuel cells and photovoltaic (PV) panels [8].

Modern aircraft, exemplified by the Boeing 787 and Airbus A380, have adopted advanced electrification, setting the stage for fully electric propulsion systems [9]. However, onboard DCMGs in MEAs may face significant voltage instability due to the following two primary factors.

1) Frequent plugging-in/-out of RESs and BESSs: In a MEA, battery packs or fuel cells may be temporarily plugged out to extend their lifespan during periods of low power demand, while PV arrays installed on the aircraft's surface may be intermittently disabled due to shading effects caused by flight maneuvers or cloud cover [10]. Additionally, emergency power reallocation may require rerouting stored energy from supercapacitors to critical flight control systems during rapid load fluctuations or fault conditions [11]. Conversely, power sources must be plugged in during peak power demand to maintain system reliability, as seen in onboard fuel cells supplementing battery-driven propulsion [12]. These plugging-in/-out events alter the number of power sources and the coupling between interconnection lines, leading to severe voltage fluctuations [13]–[15].

2) Nonlinear constant power loads (CPLs): Many critical onboard loads in MEA systems, including avionics systems, flight control actuators, electric environmental control systems, and electrically driven propulsion, can be classified as CPLs [16], [17]. CPLs inherently exhibit nonlinear and negative impedance behavior, originating from their tendency to maintain constant power consumption irrespective of voltage fluctuations. Specifically, as the voltage decreases, the load current increases in a nonlinear manner, introducing a destabilizing feedback mechanism that significantly degrades voltage stability

[18]. This adverse interaction imposes a non-intuitive and demanding load condition on the power distribution system, thereby complicating voltage control. Therefore, CPLs substantially heighten the risk of voltage collapse, particularly under high-power or transient operating conditions. Given these challenges, the problem of voltage stabilization under plugging-in/-out operations and CPLs has become a critical focus in recent research.

Significant efforts have been devoted to developing plug-n-play (PnP) voltage control strategies to address the challenges from frequent plugging-in/-out operations in DCMGs. For instance, Wang et al. [19] proposed a reliable PnP voltage control scheme for DCMGs, which employs a structured free-weight matrix to ensure seamless attachment and detachment of various power sources (e.g., BESSs/RESs). Similarly, techniques such as structured storage functions [20], [21] and structured slack matrices [22], [23] were introduced to facilitate smooth insertion and extraction of BESSs and RESs. Furthermore, a power-buffer-based PnP voltage control strategy was developed to enable flexible plugging-in/-out operations [24]. While these PnP control methods enhance system scalability for plug-in/-out operations, they are primarily designed for general DCMGs and do not explicitly address onboard MEA systems. Furthermore, CPL-induced nonlinearities can compromise their scalable effectiveness in managing dynamic addition and removal of BESSs and RESs.

A substantial body of researches on onboard DCMGs for MEA systems have predominantly focused on voltage regulation under CPLs. For example, a sliding mode finite-time control strategy was developed to achieve fast voltage regulation in MEA DCMGs with CPLs [25]. An improved power-sharing approach between BESSs and RESs was proposed to minimize power losses in DCMGs for MEA [26]. A robust voltage control method was designed for MEA DCMGs, with its performance evaluated under fault conditions [27]. Additionally, a centralized observer-based control scheme was introduced for onboard DCMGs in MEA, demonstrating that regulating voltage decreases the need for passive capacitance [28]. To enhance voltage stability in MEA DCMGs with CPLs, a neural network-based MPC framework was utilized in [29], while an adaptive backstepping control strategy was designed in [30]. Although these methods effectively address the challenges posed by nonlinear CPLs in onboard DCMGs for MEA, they do not fully account for the transient effects caused by dynamic disconnection and reconnection of power sources, which are critical in MEA applications.

Building on the insights discussed above, this study aims to tackle the following critical challenges:

1) How to establish a unified onboard DCMG model that accurately captures the complexities of real-world MEA systems?
2) How to design a new control strategy that ensures seamless plugging-in/-out operations of BESSs and RESs under CPLs?
3) What theoretical stability and performance guarantees can be provided for the proposed control scheme under dynamic operating conditions?

TABLE I

Comparative Analysis Between the Contributions of this Paper and the Existing Results in the Literature

Reference	AMEA[1]	EPnPO[2]	OUCPL[3]	AEPnPO[4]
[8]	✗	✗	✗	–
[2]	✓	✗	✗	–
[19]	✗	✓	✗	SFWM[5]
[20]	✗	✓	✗	SSF[6]
[21]	✗	✓	✗	SSF
[23]	✗	✓	✗	SSM[7]
[24]	✗	✓	✗	PB[8]
[25]–[30]	✓	✗	✓	–
This paper	✓	✓	✓	SSF

[1]Application in more electric aircraft.
[2]Ensuring plug-n-play operations.
[3]Operating under constant power loads.
[4]Approach for enabling plug-n-play operations.
[5]Structured free-weight matrix.
[6]Structured storage function.
[7]Structured slack matrix. [8]Power buffer.

To address these challenges, this study proposes a new PnP voltage control of onboard DCMGs for MEA under CPLs, enabling seamless integration and isolation of BESSs and RESs. In comparison to the existing studies, which predominantly focus on either plugging-in/-out operations without specific adaptation in MEA or CPL-induced instability of MEA, the proposed approach comprehensively addresses both issues within the context of MEA applications. A detailed comparative analysis with existing methodologies is presented in Table I. The primary contributions of this paper are outlined as follows:

1) A unified onboard DCMG model for MEA is developed to address the limitations of existing approaches by simultaneously capturing the nonlinear behavior of CPLs and the dynamic coupling effects of plugging-in/unplugging operations. The model introduces a flexible modeling paradigm for multi-bus, multi-source onboard DCMGs with multiple CPLs in MEAs. It also establishes a rigorous theoretical foundation for stability analysis and controller design.
2) A novel PnP voltage control strategy is proposed by leveraging a structured storage function technique. The method transforms interconnection couplings into a Laplacian structure of the admittance matrix, enabling a systematic stability analysis. Sufficient conditions are derived to guarantee the dissipative voltage stability of both local and global onboard DCMGs for MEA.
3) The proposed PnP control scheme is inherently scalable, operating independently of both the number of

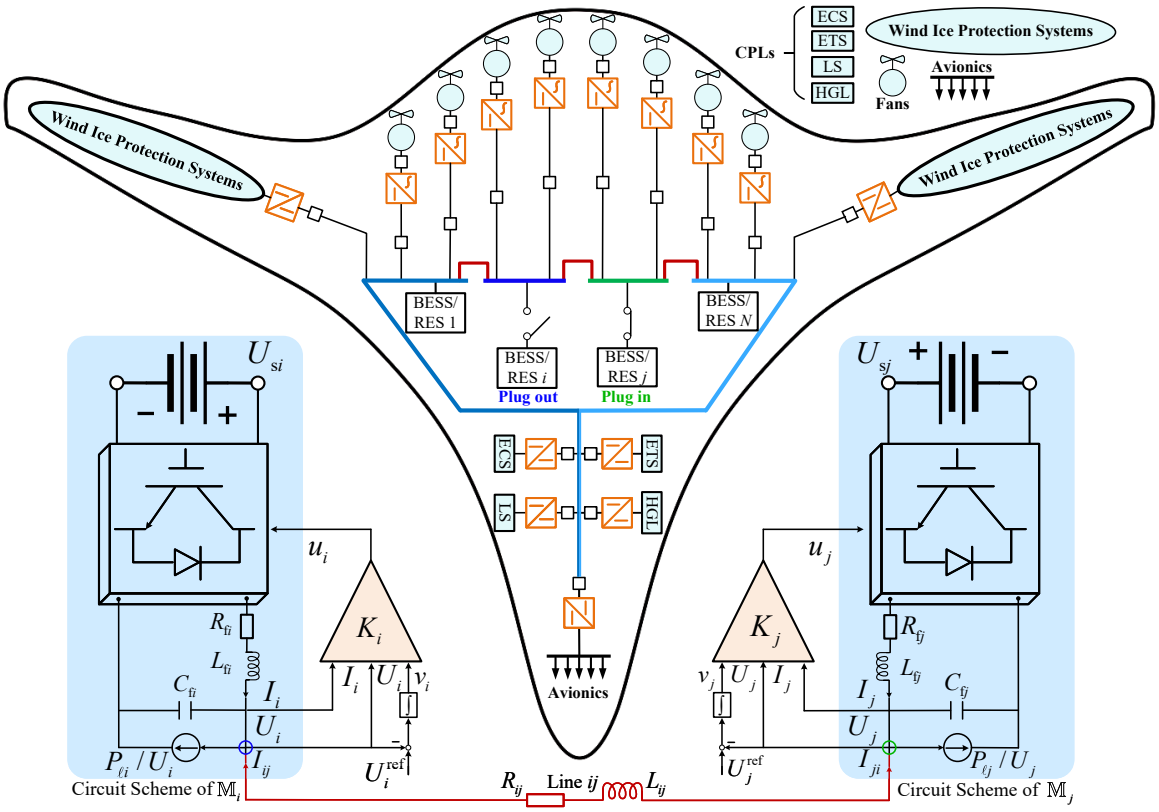

Fig. 1. A typical decentralized architecture (thick black line) and its electrical scheme (blue background) of MEAs with multi-bus DCMGs.

power sources (BESSs and RESs) and the coupling effects of interconnection lines, even under continuous addition and removal of these power sources with CPLs. Moreover, it ensures voltage stability under dynamic changes in CPL power and reference voltage while maintaining reliable operation during fault events.

The organization of this paper is as follows. Section II details the onboard DCMG model for MEA. Section III provides the dissipative stability analysis and introduces the design of a PnP voltage controller. Section IV describes the smooth plugging-in/-out operations. Section V presents the simulation results. Section VI concludes this work.

Notations: The set of all real-valued matrices of dimension $q \times r$ is denoted by $\mathbb{R}^{q\times r}$, and the zero matrix of the same dimension is written as $\mathbf{0}^{q\times r}$. The identity matrix of size l is denoted by $\mathbb{I}_l \in \mathbb{R}^{l\times l}$, and the vector $\mathbf{1}_l \in \mathbb{R}^l$ denotes a column vector with all entries equal to one. A matrix $F \in \mathbb{R}^{q\times q}$ is said to be negative definite (or positive definite) if $F < 0$ (or $F > 0$), respectively. The symbol $*$ represents the symmetric part of a matrix expression. The transpose of a matrix E is denoted by E^T. For a vector $z \in \mathbb{R}^q$, the notation $\mathrm{diag}\{z\} \in \mathbb{R}^{q\times q}$ refers to a diagonal matrix whose diagonal entries are the components of z, with all off-diagonal elements being zero.

II. SYSTEM MODELING OF ONBOARD DCMG FOR MEA

Graph Theory: The information flow within a system is modeled as the undirected graph $\mathcal{G} = (\mathcal{V}, \mathcal{E}, \mathcal{A})$. Here, $\mathcal{V} = \{1, 2, ..., n\}$ signifies the vertex set, $\mathcal{E} \subset \mathcal{V} \times \mathcal{V}$ defines the collection of edges, and $\mathcal{A} = [a_{ij}] \in \mathbb{R}^{n\times n}$ stands for the adjacency matrix. For any vertex $i \in \mathcal{V}$, the condition $a_{ii} = 0$ reflects the local flow of information. Each directed edge (j, i) in the graph is associated with a weight a_{ij}, where $a_{ij} > 0$ if $(j, i) \in \mathcal{E}$, and $a_{ij} = 0$ otherwise. The neighborhood of vertice i is denoted by $\mathcal{N}_i$. The in-degree matrix $\mathcal{D}$ is constructed as a diagonal matrix, with each diagonal entry $d_i = \sum_{j\in\mathcal{N}_i} a_{ij}$. The Laplacian matrix can be represented by $\mathcal{L} = \mathcal{D} - \mathcal{A}$.

A. Subsystem Model of Onboard DCMGs for MEA

As illustrated in the upper central part of Fig. 1 (i.e., the aircraft outline with a thick black line), a typical decentralized architecture of an MEA is depicted, comprising multi-bus onboard DCMGs linked via DC power lines. A simplified circuit diagram and control architecture of each MEA subsystem are represented by the blue background in Fig. 1. In this architecture, DC-DC converters serve as the interface for power sources, regulating power delivery to CPLs. Specifically, CPLs encompass the wing ice protection system, avionics, environmental control system (ECS), e-taxi system (ETS), lighting system (LS), as well as hotel and galley loads (HGL).

For analytical simplicity, the local CPL is positioned at the point of common coupling (PCC), and the interconnection of loads can be mapped to this topology using Kron reduction, even if the load bus is located elsewhere [31]. The ideal DC voltage source representation for RESs is justified by the fact that power variations in BESSs and RESs typically evolve over timescales significantly slower than those governing voltage dynamics in stability analysis [25]. In addition, these RESs are commonly interfaced via power electronic converters equipped with inner control loops and local BESSs, which effectively mitigate short-term power fluctuations and enable the aggregated system behavior to be approximated as a controllable voltage source [13]. Power lines are assumed to comply with the quasi-stationary line (QSL) approximation, which implies that the current between subsystems is given by $I_{ij} = (U_j - U_i)/R_{ij}$ and ensures neutral interaction among power sources [32].

By utilizing Kirchhoff's voltage and current laws on the circuit scheme depicted in Fig. 1, where an integrator is included to eliminate static voltage tracking errors, the subsystem dynamics are formulated as

$$\begin{cases} \dot{U}_i = \dfrac{1}{C_{\mathrm{f}i}} I_i + \displaystyle\sum_{j\in\mathcal{N}_i} \frac{1}{C_{\mathrm{f}i} R_{ij}}(U_j - U_i) - \frac{1}{C_{\mathrm{f}i}} \frac{P_{\ell i}}{U_i}, \\ \dot{I}_i = -\dfrac{1}{L_{\mathrm{f}i}} U_i - \dfrac{R_{\mathrm{f}i}}{L_{\mathrm{f}i}} I_i + \dfrac{U_{\mathrm{s}i}}{L_{\mathrm{f}i}} d_i, \\ \dot{v}_i = U_{\mathrm{ref}i} - U_i, \end{cases} \tag{1}$$

where U_i and U_j $(i \in \mathcal{V}, j \in \mathcal{N}_i)$ represent the voltage signals of subsystems i and j, respectively. $U_{\mathrm{ref}i}$ stands for the reference voltage, and $U_{\mathrm{s}i}$ defines the voltage generated by the BESS/RES. The electrical elements of the RLC filter are described by $R_{\mathrm{f}i}$, $L_{\mathrm{f}i}$, and $C_{\mathrm{f}i}$, while I_i represents the current flowing through the filter. The parameter R_{ij} characterizes the resistance of the power line connecting subsystems i and j. Additionally, $P_{\ell i}$ corresponds to the CPL demand. The duty cycle, denoted by $d_i \in [0, 1]$, regulates the system operation, and v_i is the integral of the error between $U_{\mathrm{ref}i}$ and U_i.

Remark 1: The inherent nonlinear and negative impedance behavior of CPLs is explicitly captured in the system model. In MEA microgrids, CPLs are modeled to draw constant power regardless of voltage fluctuations, typically expressed as $P_{\ell i} = U_i I_{\ell i} =$ constant, where $I_{\ell i}$ denotes the load current. Rearranging this yields $I_{\ell i} = P_{\ell i}/U_i$, which reveals a hyperbolic relationship between current and voltage. As voltage decreases, the corresponding current increases nonlinearly, implying a negative incremental impedance characteristic, i.e., $\partial U_i/\partial I_{\ell i} < 0$. This behavior manifests in the system dynamics (1) through the nonlinear term $P_{\ell i}/U_i$, which introduces a destabilizing feedback loop that amplifies voltage deviations and compromises system stability.

For a given equilibrium $[\widetilde{U}_i, \widetilde{U}_j, \widetilde{I}_i, \widetilde{v}_i, \widetilde{d}_i, \widetilde{U}_{\mathrm{ref}i}]$, the constant power demand $P_{\ell i}$ must remain below a maximum allowable value, which can be determined by linearizing (1) at the operating point. This maximum bound ensures that the Jacobian matrix of (1) is Hurwitz, guaranteeing the existence of a stable equilibrium [13]. Since the CPL term $P_{\ell i}/U_i$ is inherently nonlinear, the stability of (1) is not automatically ensured. To effectively apply Lyapunov-based methods, the dynamics are reformulated so that the equilibrium is shifted to the origin. This can be achieved by introducing the following coordinate transformation:

$$\begin{aligned} &\overline{U}_i = U_i - \widetilde{U}_i, \overline{U}_j = U_j - \widetilde{U}_j, \overline{I}_i = I_i - \widetilde{I}_i, \\ &\overline{v}_i = v_i - \widetilde{v}_i, \overline{d}_i = d_i - \widetilde{d}_i, \overline{U}_{\mathrm{ref}i} = U_{\mathrm{ref}i} - \widetilde{U}_{\mathrm{ref}i}, \end{aligned}$$

the local dynamics of MEA are derived as follows:

$$\begin{cases} \dot{\overline{U}}_i = \dfrac{1}{C_{\mathrm{f}i}} \overline{I}_i + \displaystyle\sum_{j\in\mathcal{N}_i} \frac{1}{C_{\mathrm{f}i} R_{ij}}(\overline{U}_j - \overline{U}_i) - \frac{1}{C_{\mathrm{f}i}} f_i(\overline{U}_i), \\ \dot{\overline{I}}_i = -\dfrac{1}{L_{\mathrm{f}i}} \overline{U}_i - \dfrac{R_{\mathrm{f}i}}{L_{\mathrm{f}i}} \overline{I}_i + \dfrac{U_{\mathrm{s}i}}{L_{\mathrm{f}i}} \overline{d}_i, \\ \dot{v}_i = \overline{U}_{\mathrm{ref}i} - \overline{U}_i, \end{cases} \tag{2}$$

where $f_i(\overline{U}_i) = \frac{P_{\ell i}\overline{U}_i}{\widetilde{U}_i(\overline{U}_i + \widetilde{U}_i)}$.

Consequently, the subsystem dynamics are captured by the following state-space framework:

$$\mathbb{M}_i : \begin{cases} \dot{x}_i(t) = A_{ii}x_i(t) + B_i u_i(t) + W_i w_i(t) \\ \qquad\quad + H_i f_i\big(x_i(t)\big) + \displaystyle\sum_{j\in\mathcal{N}_i} A_{ij}\big(x_j(t) - x_i(t)\big), \\ y_i(t) = D_i x_i(t), \end{cases} \tag{3}$$

where $x_i = \left[\overline{U}_i, \overline{I}_i, \overline{v}_i\right]^T$ represents the state vector of subsystem $\mathbb{M}_i$ and x_j denotes the state vector of subsystem $\mathbb{M}_j$. The control signal is denoted by $u_i = \overline{d}_i$. $w_i = \overline{U}_{\mathrm{ref}i}$ indicates the external disturbance. $f_i(x_i)$ denotes the nonlinearity of the CPL. Additionally, the term $\sum_{j\in\mathcal{N}_i} A_{ij}(x_j(t) - x_i(t))$ represents the coupling of power line between $\mathbb{M}_i$ and $\mathbb{M}_j$, where A_{ij} denotes the coupling matrix. The matrices of the local DCMG for MEA are given as

$$A_{ii} = \begin{bmatrix} 0 & \frac{1}{C_{\mathrm{f}i}} & 0 \\ -\frac{1}{L_{\mathrm{f}i}} & -\frac{R_{\mathrm{f}i}}{L_{\mathrm{f}i}} & 0 \\ -1 & 0 & 0 \end{bmatrix}, A_{ij} = \begin{bmatrix} \frac{1}{R_{ij}C_{\mathrm{f}i}} & 0 & 0 \\ 0 & 0 & 0 \\ 0 & 0 & 0 \end{bmatrix},$$

$$B_i = \begin{bmatrix} 0 \\ \frac{U_{\mathrm{s}i}}{L_{\mathrm{f}i}} \\ 0 \end{bmatrix}, W_i = \begin{bmatrix} 0 \\ 0 \\ 1 \end{bmatrix}, H_i = \begin{bmatrix} -\frac{1}{C_{\mathrm{f}i}} \\ 0 \\ 0 \end{bmatrix}, D_i = \mathbb{I}_3.$$

B. Decentralized Control Architecture

Before designing the controller, the controllability condition for the subsystem is established.

Proposition 1: The state-space pair (A_{ii}, B_i) exhibits complete controllability.

Proof: Constructing the controllability matrix yields

$$\begin{aligned} \mathcal{M}_i &= \begin{bmatrix} B_i & A_{ii}B_i & A_{ii}^2 B_i \end{bmatrix} \\ &= \begin{bmatrix} 0 & \frac{U_{\mathrm{s}i}}{L_{\mathrm{f}i}C_{\mathrm{f}i}} & -\frac{R_{\mathrm{f}i}U_{\mathrm{s}i}}{L_{\mathrm{f}i}^2 C_{\mathrm{f}i}} \\ \frac{U_{\mathrm{s}i}}{L_{\mathrm{f}i}} & -\frac{R_{\mathrm{f}i}U_{\mathrm{s}i}}{L_{\mathrm{f}i}^2} & \frac{R_{\mathrm{f}i}^2 U_{\mathrm{s}i}C_{\mathrm{f}i} - U_{\mathrm{s}i}L_{\mathrm{f}i}}{L_{\mathrm{f}i}^3 C_{\mathrm{f}i}} \\ 0 & 0 & -\frac{U_{\mathrm{s}i}}{L_{\mathrm{f}i}C_{\mathrm{f}i}} \end{bmatrix}. \end{aligned}$$

TABLE II
Comparison of Control Architectures for Onboard DCMGs in MEA

Feature	Centralized Control	Distributed Control	Decentralized Control
Network Communication	Global communication via central controller	Neighbor-to-neighbor communication	Independent of communication networks
Scalability	Poor; PnP requires central controller update and full network reconfiguration	Limited; PnP requires distributed controller update and network reconfiguration	Fully scalable; PnP without controller update or network reconfiguration
Resilience	Single point of failure	Improved fault tolerance; still communication-dependent	Robust to cyber threats, packet losses, and network delays; simple local implementation
Privacy	Full disclosure of all subsystem states and parameters	Partial privacy; neighbor states shared	Full privacy; no model or state disclosure
Redundancy	Possible but requires centralized coordination	Possible with communication overhead	Built-in capability for redundant supply paths with minimal coordination
Complexity	High; global monitoring and control logic required	Moderate; needs communication protocols and synchronization	Low; based solely on local measurements
Application	Small-scale or fully supervised systems	Medium-scale microgrids with coordinated controllers	Suitable for safety-critical, privacy-sensitive, or bandwidth-constrained MEA applications

Given that all electrical components in onboard MEA DCMGs are positive-valued, the controllability matrix $\mathcal{M}_i$ is full rank, i.e., $\text{rank}(\mathcal{M}_i) = 3$, thereby satisfying the controllability condition.

Based on the controllability analysis given in Proposition 1, we formulate the local control law for $\mathbb{M}_i$ (3) as

$$\mathbb{C}_i : u_i(t) = K_i x_i(t), \tag{4}$$

where $K_i \in \mathbb{R}^{1\times 3}$ denotes the controller gain matrix, whose design method is detailed in Section III.

Remark 2: Control architectures in onboard DCMGs for MEA can be generally categorized as centralized, distributed, or decentralized [6]. A detailed side-by-side comparison of these architectures is summarized in Table II. Specifically, centralized control can achieve optimal power management but suffers from poor scalability, high implementation complexity, single points of failure, and privacy issues. Distributed control mitigates some risks via local coordination; however, it remains susceptible to network-induced delays, packet losses, and security vulnerabilities, as well as still requires access to neighboring states, which limits scalability and adds moderate communication overhead. In contrast, the proposed fully decentralized control operates independently of communication networks, enabling scalable PnP operations without the need for controller update or network reconfiguration. It also reduces implementation complexity by relying solely on local measurements, enhances resilience against network-induced problems, preserves privacy by avoiding model disclosure, and offers built-in redundancy with minimal coordination [33]. Therefore, decentralized control is particularly suitable for safety-critical, privacy-sensitive, or bandwidth-constrained MEA applications.

C. Global Model of Onboard DCMGs for MEA

The global model of MEA DCMGs, composed of n subsystems, can be described as follows:

$$\mathbf{M}_n : \begin{cases} \dot{\boldsymbol{x}}(t) = \boldsymbol{A}\boldsymbol{x}(t) + \boldsymbol{B}\boldsymbol{u}(t) + \boldsymbol{W}\boldsymbol{w}(t) + \boldsymbol{H}\boldsymbol{f}(\boldsymbol{x}(t)), \\ \boldsymbol{y}(t) = \boldsymbol{D}\boldsymbol{x}(t), \end{cases} \tag{5}$$

where

$$\begin{aligned} \boldsymbol{x}(t) &= \left[x_1^T(t), x_2^T(t), \ldots, x_n^T(t)\right]^T, \\ \boldsymbol{y}(t) &= \left[y_1^T(t), y_2^T(t), \ldots, y_n^T(t)\right]^T, \\ \boldsymbol{u}(t) &= \left[u_1^T(t), u_2^T(t), \ldots, u_n^T(t)\right]^T, \\ \boldsymbol{w}(t) &= \left[w_1^T(t), w_2^T(t), \ldots, w_n^T(t)\right]^T, \\ \boldsymbol{f}(\boldsymbol{x}(t)) &= \left[f_1^T(x_1(t)), f_2^T(x_2(t)), \ldots, f_n^T(x_n(t))\right]^T, \end{aligned}$$

and

$$\boldsymbol{A} = \begin{bmatrix} A_{11}+A_{d1} & A_{12} & \cdots & A_{1n} \\ A_{21} & A_{22}+A_{d2} & \cdots & A_{2n} \\ \vdots & \vdots & \ddots & \vdots \\ A_{n1} & A_{n2} & \cdots & A_{nn}+A_{dn} \end{bmatrix},$$

$$\boldsymbol{B} = \text{diag}\left\{B_1, B_2, \ldots, B_n\right\}, \boldsymbol{H} = \text{diag}\left\{H_1, H_2, \ldots, H_n\right\},$$
$$\boldsymbol{W} = \text{diag}\left\{W_1, W_2, \ldots, W_n\right\}, \boldsymbol{D} = \text{diag}\left\{D_1, D_2, \ldots, D_n\right\}.$$

The matrix $\boldsymbol{A}$ can be decomposed into three components as

$$\boldsymbol{A} = \boldsymbol{A}_v + \boldsymbol{A}_d + \boldsymbol{A}_a, \tag{6}$$

where $\boldsymbol{A}_v = \text{diag}\left\{A_{11}, A_{22}, \ldots, A_{nn}\right\}$ captures the dynamics of each subsystem of MEA. Both matrices $\boldsymbol{A}_d$ and $\boldsymbol{A}_a$ denote the interconnections of power lines among BESSs/RESs. Specifically, the matrix $\boldsymbol{A}_d = \text{diag}\left\{A_{d1}, A_{d2}, \ldots, A_{dn}\right\}$ captures the local state dependencies on adjacent subsystems and is structured in block

form as

$$A_{di} = \begin{bmatrix} -\sum_{j\in\mathcal{N}_i} \frac{1}{R_{ij}C_{\mathrm{fi}}} & \mathbf{0}^{1\times 2} \\ \hdashline \mathbf{0}^{2\times 1} & \mathbf{0}^{2\times 2} \end{bmatrix}. \tag{7}$$

The matrix $\boldsymbol{A}_a$ embodies the inter-subsystem interactions and exhibits a sparse structure, with zero diagonal blocks and non-zero off-diagonal elements A_{ij} $(j \neq i)$.

To establish the theoretical foundation for the subsequent analysis, the following lemmas and definition are introduced.

Lemma 1 [34]: For any real matrices X_1 and X_2, there exists a positive scalar ϕ satisfying the following inequality:

$$X_1^T X_2 + X_2^T X_1 \leq \phi X_1^T X_1 + \phi^{-1} X_2^T X_2.$$

Lemma 2 [35]: For a nonlinear dynamical plant characterized by a Lipschitz continuous vector field $f(x(t))$, one can find a scalar $\phi > 0$ and a constant matrix G satisfying

$$f^T(x(t))f(x(t)) \leq \phi x^T(t) G^T G x(t). \tag{8}$$

Lemma 3 [36]: The Laplacian matrix of an undirected graph is symmetric and positive semidefinite.

Proof: Based on the definitions in Graph Theory, the Laplacian matrix is defined as $\mathcal{L} = \mathcal{D} - \mathcal{A}$, where $\mathcal{D}$ is the diagonal degree matrix and $\mathcal{A}$ is the adjacency matrix of the undirected graph $\mathcal{G}$. Since both $\mathcal{D}$ and $\mathcal{A}$ are symmetric, it follows that $\mathcal{L}$ is symmetric as well.

To establish the positive semidefiniteness of $\mathcal{L}$, consider the standard quadratic form:

$$\delta^T \mathcal{L} \delta = \sum_{(i,j)\in\mathcal{E}} a_{ij}(\delta_i - \delta_j)^2 \geq 0, \ \forall \delta \in \mathbb{R}^n,$$

where a_{ij} denotes the edge weight. Since the expression is a sum of non-negative terms, it follows that $\mathcal{L}$ is positive semidefinite. Alternatively, the Laplacian can be factorized as $\mathcal{L} = JJ^T$, where J denotes the vertex-edge incidence matrix of the graph $\mathcal{G}$. This factorization implies:

$$\delta^T \mathcal{L} \delta = \delta^T J J^T \delta = \left\| J^T \delta \right\|^2 \geq 0,$$

further confirming that $\mathcal{L}$ is positive semidefinite. Thus, $\mathcal{L}$ is both symmetric and positive semidefinite, which concludes the proof.

Definition 1 [37]: A dynamical system $\mathbb{M}_i$ is said to be dissipative with respect to the energy supply rate $\mathscr{S}(y_i(t), w_i(t))$ if there exists a non-negative storage function $V_i(x_i(t))$ such that, for all $t > t_0 \geq 0$

$$V_i(x_i(t)) - V_i(x_i(t_0)) \leq \int_{t_0}^{t} \mathscr{S}(y_i(\tau), w_i(\tau)) d\tau.$$

If the supply rate takes the following quadratic form:

$$\mathscr{S}(y_i(\tau), w_i(\tau)) = y_i^T(\tau) Q_i y_i(\tau) + 2 y_i^T(\tau) S_i w_i(\tau) + w_i^T(\tau) R_i w_i(\tau),$$

the system is termed QSR-dissipative, where "QSR" denotes the triple of real matrices (Q_i, S_i, R_i). Specifically, $Q_i = Q_i^T \in \mathbb{R}^{3\times 3}$ weights the output y_i, $R_i = R_i^T \in \mathbb{R}$ weights the scalar disturbance w_i, and $S_i \in \mathbb{R}^{3\times 1}$ captures the cross-effect between the output and disturbance. Matrices (Q_i, S_i, R_i) collectively determine the dissipation characteristics of the system.

Remark 3: QSR-dissipativity provides a unifying framework to capture a broad range of dynamical properties by appropriate selections of the weighting matrices Q_i, S_i, and R_i. In particular, the local MEA system $\mathbb{M}_i$ (3) satisfying Definition 1 exhibits the following classical behaviors:

1) *Passive:* If $Q_i = 0$, $S_i = \frac{1}{2}\mathbf{1}_3$, and $R_i = 0$.
2) *Strictly passive:* If $Q_i = \xi_1 \mathbb{I}_3$, $S_i = \frac{1}{2}\mathbf{1}_3$, and $R_i = -\mu_1$, where both ξ_1 and μ_1 are positive scalars.
3) *$\mathcal{L}_2$ stable:* If $Q_i = -\frac{1}{\xi_2}\mathbb{I}_3$, $S_i = 0$, and $R_i = \xi_2$, where $\xi_2 > 0$ corresponds to the $\mathcal{L}_2$-gain bound of the system.
4) *Conic:* If $Q_i = -\mathbb{I}_3$, $S_i = \delta_1 \mathbf{1}_3$, and $R_i = \mu_2^2 - \delta_1^2$, where μ_2 is a positive scalar and δ_1 is an arbitrary scalar. Notably, when $\delta_1 = 0$, the conic condition degenerates into the standard H_∞ performance case.
5) *Sector-bounded:* If $Q_i = -\mathbb{I}_3$, $S_i = \frac{\delta_2+\delta_3}{2}\mathbf{1}_3$, and $R_i = -\delta_2\delta_3$, where both δ_2 and δ_3 are arbitrary scalars, which define the sector bounds.

III. DISSIPATIVE STABILITY ANALYSIS AND PNP VOLTAGE CONTROLLER DESIGN

This section establishes dissipative voltage stability conditions for the MEA subsystem $\mathbb{M}_i$ (3), initially neglecting the line coupling term $\sum_{j\in\mathcal{N}_i} A_{ij}(x_j(t) - x_i(t))$. Next, the coupling effects in the global MEA $\mathbf{M}_n$ (5) are removed. Finally, a method for designing the PnP voltage controller is presented.

Theorem 1: Given a positive scalar ϕ_i and a matrix G_i, the local MEA subsystem $\mathbb{M}_i$, excluding line couplings, is QSR-dissipative if there exist matrices K_i, S_i, symmetric matrices Q_i, R_i, and a positive definite matrix P_i such that the following local condition is satisfied:

$$\Pi_i = \begin{bmatrix} \Pi_i^{11} & P_i W_i - S_i & P_i H_i & G_i^T \\ * & -R_i & 0 & 0 \\ * & * & -\phi_i & 0 \\ * & * & * & -\phi_i^{-2} \end{bmatrix} < 0, \tag{9}$$

where $\Pi_i^{11} = P_i A_{ii} + A_{ii}^T P_i + P_i B_i K_i + K_i^T B_i^T P_i - Q_i$.

Proof: Consider the following candidate storage function:

$$V_i(t) = x_i^T(t) P_i x_i(t). \tag{10}$$

By computing the time derivative of $V_i(t)$, we obtain

$$\begin{aligned} \dot{V}_{1i}(t) =& x_i^T(t) \big(P_i A_{ii} + A_{ii}^T P_i \\ &+ P_i B_i K_i + K_i^T B_i^T P_i \big) x_i(t) \\ &+ 2 x_i^T(t) P_i W_i w_i(t) + 2 x_i^T(t) P_i H_i f_i(x_i(t)). \end{aligned} \tag{11}$$

Consider the nonlinear term $2x_i^T(t) P_i H_i f_i(x_i(t))$. By applying Lemma 1, which states that for arbitrary real matrices $X_1 = f_i(x_i(t))$ and $X_2 = x_i^T(t) P_i H_i$, there

exists a positive scalar $\phi_i > 0$ such that

$$2x_i^T(t)P_iH_if_i(x_i(t)) \le \phi_i f_i^T(x_i(t))f_i(x_i(t)) + \phi_i^{-1}x_i^T(t)P_iH_iH_i^TP_ix_i(t). \quad (12)$$

Next, applying Lemma 2, which asserts that if the nonlinear function $f_i(x_i(t))$ is Lipschitz continuous, then there exists a constant matrix G_i and a scalar ϕ_i such that

$$f_i^T(x_i(t))f_i(x_i(t)) \le \phi_i x_i^T(t)G_i^TG_ix_i(t). \quad (13)$$

Substituting the above inequality into Eq. (12) yields

$$\begin{aligned} &2x_i^T(t)P_iH_if_i(x_i(t)) \\ &\le \phi_i f_i^T(x_i(t))f_i(x_i(t)) + \phi_i^{-1}x_i^T(t)P_iH_iH_i^TP_ix_i(t) \\ &\le \phi_i^2 x_i^T(t)G_i^TG_ix_i(t) + \phi_i^{-1}x_i^T(t)P_iH_iH_i^TP_ix_i(t). \end{aligned} \quad (14)$$

For any bounded non-zero disturbance $w_i(t)$, define the performance index as

$$\mathcal{J}_i(\tau) = \int_0^\tau \begin{bmatrix} y_i(t) \\ w_i(t) \end{bmatrix}^T \begin{bmatrix} Q_i & S_i \\ * & R_i \end{bmatrix}^T \begin{bmatrix} y_i(t) \\ w_i(t) \end{bmatrix} dt. \quad (15)$$

Then, under the zero initial condition $x_{i0} = 0$, combining (11)–(15) yields the following expression:

$$\begin{aligned} \mathcal{J}_i^\star &= V_i(x_i(\tau)) - J_i(\tau) = \int_0^\tau \Big\{\dot{V}_i(x_i(t)) - y_i^T(t)Q_iy(t) \\ &\quad - 2y_i^T(t)S_iw_i(t) - w_i^T(t)R_iw_i(t)\Big\}dt \\ &= \int_0^\tau \left\{\zeta_i^T(t)\Sigma_i\zeta_i(t)\right\}dt, \end{aligned} \quad (16)$$

where

$$\Sigma_i = \begin{bmatrix} \Pi_i^{11} + \phi_i^{-1}P_iH_iH_i^TP_i + \phi_i^2G_i^TG_i & P_iW_i - S_i \\ * & -R_i \end{bmatrix} \quad (17)$$

and $\zeta_i(t) = \left[x_i^T(t), w_i^T(t)\right]^T$.

By applying Schur complement to Σ_i (17), it can be obtained that Σ_i is equivalent to Π_i. Therefore, $\Pi_i < 0$ implies $\mathcal{J}_i^\star < 0$, which guarantees the QSR-dissipativity of DCMGs for MEA as defined in Definition 1.

Remark 4: Note that Theorem 1 establishes a sufficient condition to ensure the QSR-dissipative voltage stability of the local MEA DCMG model under the assumption of no line couplings. However, in a practical MEA, the frequent addition and disconnection of BESSs and RESs continuously alter both the number of power sources and their interconnection couplings. For instance, the addition of a PV array increases the number of power sources and changes line couplings, while disconnecting a battery pack, either for maintenance or to extend its lifespan, reduces the number of power sources and reshapes the system couplings. These plugging-in/unplugging operations induce significant voltage fluctuations, making it essential to consider line couplings to ensure overall system stability. Therefore, condition (9) alone is insufficient, necessitating a PnP control method independent of other power sources and power lines.

The following theorem addresses the issue highlighted in Remark 4 and provides a formal solution.

Theorem 2: Given positive scalars $\hat{p}, \phi_i$ and a matrix $\boldsymbol{G}$, the global MEA $\mathbf{M}_n$ interconnected via power lines is QSR-dissipative if there exist matrices $\boldsymbol{K}, \boldsymbol{S}, \boldsymbol{Q}, \boldsymbol{R}$ and a positive definite matrix $\boldsymbol{P}$ with the block entry P_i defined as

$$P_i = \begin{bmatrix} \hat{p}C_{\mathrm{f}i} & \mathbf{0}^{1\times 2} \\ \mathbf{0}^{2\times 1} & \tilde{P}_i \end{bmatrix}, \ \tilde{P}_i > 0, \quad (18)$$

provided that the following global condition is satisfied:

$$\boldsymbol{\Pi} = \begin{bmatrix} \boldsymbol{\Pi}^{11} & \boldsymbol{PW - S} & \boldsymbol{PH} & \boldsymbol{G}^T \\ * & -\boldsymbol{R} & 0 & 0 \\ * & * & -\boldsymbol{\Phi} & 0 \\ * & * & * & -\boldsymbol{\Phi}^{-2} \end{bmatrix} < 0, \quad (19)$$

where $\boldsymbol{\Phi} = \mathrm{diag}\{\phi_1, \phi_2, \ldots, \phi_n\}$ is a constant diagonal matrix and

$$\begin{aligned} &\boldsymbol{\Pi}^{11} = \boldsymbol{PA} + \boldsymbol{A}^T\boldsymbol{P} + \boldsymbol{PBK} + \boldsymbol{K}^T\boldsymbol{B}^T\boldsymbol{P} - \boldsymbol{Q}, \\ &\boldsymbol{G} = \mathrm{diag}\{G_1, G_2, \ldots, G_n\}, \boldsymbol{K} = \mathrm{diag}\{K_1, K_2, \ldots, K_n\}, \\ &\boldsymbol{S} = \mathrm{diag}\{S_1, S_2, \ldots, S_n\}, \boldsymbol{Q} = \mathrm{diag}\{Q_1, Q_2, \ldots, Q_n\}, \\ &\boldsymbol{R} = \mathrm{diag}\{R_1, R_2, \ldots, R_n\}, \boldsymbol{P} = \mathrm{diag}\{P_1, P_2, \ldots, P_n\}. \end{aligned}$$

Proof: From $\boldsymbol{A} = \boldsymbol{A}_v + \boldsymbol{A}_d + \boldsymbol{A}_a$ in (6), it follows that

$$\boldsymbol{\Pi} = \boldsymbol{\Pi}_v + \boldsymbol{\Pi}_c, \quad (20)$$

where $\boldsymbol{\Pi}_v$ represents the internal energy dissipativity of all MEA subsystems without line couplings, while $\boldsymbol{\Pi}_c$ denotes the negative coupling effects of power lines, expressed as

$$\boldsymbol{\Pi}_v = \begin{bmatrix} \boldsymbol{\Pi}_v^{11} & \boldsymbol{PW - S} & \boldsymbol{PH} & \boldsymbol{G}^T \\ * & -\boldsymbol{R} & 0 & 0 \\ * & * & -\boldsymbol{\Phi} & 0 \\ * & * & * & -\boldsymbol{\Phi}^{-2} \end{bmatrix}, \quad (21)$$

and

$$\boldsymbol{\Pi}_c = \begin{bmatrix} \boldsymbol{\Pi}_c^{11} & \mathbf{0}^{9n\times 3n} \\ \mathbf{0}^{3n\times 9n} & \mathbf{0}^{3n\times 3n} \end{bmatrix}, \quad (22)$$

where

$$\begin{aligned} &\boldsymbol{\Pi}_v^{11} = \boldsymbol{A}_v^T\boldsymbol{P} + \boldsymbol{PA}_v + \boldsymbol{K}^T\boldsymbol{B}^T\boldsymbol{P} + \boldsymbol{PBK} - \boldsymbol{Q}, \\ &\boldsymbol{\Pi}_c^{11} = \boldsymbol{A}_d^T\boldsymbol{P} + \boldsymbol{PA}_d + \boldsymbol{A}_a^T\boldsymbol{P} + \boldsymbol{PA}_a. \end{aligned}$$

By aggregating all the local conditions (9) in Theorem 1, it can be easily obtained that

$$\boldsymbol{\Pi}_v < 0. \quad (23)$$

Clearly, the coupling matrix $\boldsymbol{\Pi}_c$ contains only one nonzero element located at position $(1,1)$, which enables the analysis to concentrate exclusively on $\boldsymbol{\Pi}_c^{11}$. Particularly, each block of the matrix $\boldsymbol{A}_d^T\boldsymbol{P} + \boldsymbol{PA}_d$ can be expressed as $A_{di}^TP_i + P_iA_{di}$ for $i = 1, 2, \ldots, n$. Moreover, each block in position (i, j) of $\boldsymbol{A}_a^T\boldsymbol{P} + \boldsymbol{PA}_a$ can be denoted as $A_{ji}^TP_j + P_iA_{ij}$ if $i \in \mathcal{V}, j \in \mathcal{N}_i$, and 0 otherwise.

Then, by considering the structural properties of matrices A_{di} (7) and P_i (18), it follows that

$$A_{di}^TP_i + P_iA_{di} = \begin{bmatrix} -\sum\limits_{j\in\mathcal{N}_i}\frac{2\hat{p}}{R_{ij}} & \mathbf{0}^{1\times 2} \\ \mathbf{0}^{2\times 1} & \mathbf{0}^{2\times 2} \end{bmatrix} \in \mathbb{R}^{3\times 3}. \quad (24)$$

It is evident that the matrix in (24) contains a single nonzero element located at position $(1,1)$, with the remaining entries in the last two rows and columns being zero. After eliminating the zero entries, define $\mathscr{L}_{ii} = -\sum_{j\in\mathcal{N}_i} 2\hat{p}/R_{ij}$ and collect these modified blocks, which yields

$$\mathcal{D} = \operatorname{diag}\{\mathscr{L}_{11},\ldots,\mathscr{L}_{ii},\ldots,\mathscr{L}_{nn}\}. \tag{25}$$

Combining matrix A_{ij} (3) and P_i (18), one obtains

$$A_{ji}^T P_j + P_i A_{ij} = \begin{bmatrix} \frac{2\hat{p}}{R_{ij}} & \mathbf{0}^{1\times 2} \\ \mathbf{0}^{2\times 1} & \mathbf{0}^{2\times 2} \end{bmatrix} \in \mathbb{R}^{3\times 3}. \tag{26}$$

It is clear that only the element in position (1,1) of (26) is nonzero. Defining $\mathscr{L}_{ij}$ represents the item after deleting the last two rows and columns of (26), we obtain $\mathscr{L}_{ij} = 2\hat{p}/R_{ij}$ if $i \in \mathcal{V}, j \in \mathcal{N}_i$, and 0 otherwise. Defining matrix $\mathcal{A}$ collects the above modified blocks, one has

$$\mathcal{A} = \begin{bmatrix} 0 & \mathscr{L}_{12} & \cdots & \mathscr{L}_{1n} \\ \mathscr{L}_{21} & 0 & \cdots & \mathscr{L}_{2n} \\ \vdots & \vdots & \ddots & \vdots \\ \mathscr{L}_{n1} & \mathscr{L}_{n2} & \cdots & 0 \end{bmatrix}. \tag{27}$$

Defining $\mathcal{L} = \mathcal{D} + \mathcal{A}$, we conclude that the definiteness (positive or negative) of $\mathbf{\Pi}_c^{11}$ can be examined via $\mathcal{L}$, with the following structure:

$$\mathcal{L} = \begin{bmatrix} \mathscr{L}_{11} & \mathscr{L}_{12} & \cdots & \mathscr{L}_{1n} \\ \mathscr{L}_{21} & \mathscr{L}_{22} & \cdots & \mathscr{L}_{2n} \\ \vdots & \vdots & \ddots & \vdots \\ \mathscr{L}_{n1} & \mathscr{L}_{n2} & \cdots & \mathscr{L}_{nn} \end{bmatrix}. \tag{28}$$

By observing the structure of $\mathcal{D}$ in (25), one knows that $-\mathcal{D}$ is identical to the definition of the in-degree matrix in Graph Theory. Similarly, the structure of $\mathcal{A}$ in (27) aligns with the adjacency matrix definition. Therefore, $-\mathcal{L}$ represents a Laplacian matrix, which implies its symmetry and positive semidefiniteness. That is to say

$$\mathcal{L} \le 0, \tag{29}$$

which is equivalent to

$$\mathbf{\Pi}_c \le 0. \tag{30}$$

Therefore, the LMI condition (19) can be derived by combining (23) and (30) under the SSF matrix P_i (18). This completes the proof.

Remark 5: Theorem 2 presents a sufficient condition to ensure QSR-dissipative voltage stability of the global MEA DCMG model $\mathbf{M}_n$, where n power sources are interconnected via power lines, with explicit consideration of line couplings. The detrimental effects arising from power line interactions, arising from the frequent integration and disconnection of BESSs and RESs, are effectively mitigated by representing these interactions through the Laplacian matrix, obtained via the structured storage function technique (18). Therefore, the stability of $\mathbf{M}_n$ is ensured if condition (19) or (23) holds, as it represents a straightforward aggregation of the local stability condition (9) for each subsystem.

However, due to the inherent complexity of conditions (9) and (19), directly parameterizing the controller gain K_i via Theorem 1 or Theorem 2 is not feasible. This limitation motivates the development of the following result.

Theorem 3: Given positive scalars $\hat{p}$, ϕ_i, and a matrix G_i, the global MEA $\mathbf{M}_n$, interconnected with n power sources via power lines, is QSR-dissipative if there exist positive scalars ζ_i, γ_i, matrices $Z_i, \hat{S}_i$, symmetric matrices $\hat{Q}_i, \hat{R}_i$, and a positive definite matrix Y_i satisfying

$$Y_i = \begin{bmatrix} \frac{1}{\hat{p}C_{Ii}} & \mathbf{0}^{1\times 2} \\ \mathbf{0}^{2\times 1} & \tilde{Y}_i \end{bmatrix} > 0,\ \tilde{Y}_i > 0, \tag{31}$$

such that the following conditions hold:

$$\Omega_i = \begin{bmatrix} \Omega_i^{11} & W_i - S_i & H_i & Y_i G_i^T \\ * & -R_i & 0 & 0 \\ * & * & -\phi_i & 0 \\ * & * & * & -\phi_i^{-2} \end{bmatrix} < 0, \tag{32}$$

$$\begin{bmatrix} -\zeta_i \mathbb{I}_3 & Z_i^T \\ * & -1 \end{bmatrix} < 0, \tag{33}$$

$$\begin{bmatrix} Y_i & \mathbf{1}_3 \\ * & \gamma_i \end{bmatrix} > 0, \tag{34}$$

where $\Omega_i^{11} = A_{ii}Y_i + Y_i A_{ii}^T + B_i Z_i + Z_i^T B_i^T - \widehat{Q}_i$.

As a result, the controller gain K_i is explicitly defined as

$$K_i = Z_i Y_i^{-1}, \tag{35}$$

and it is subject to the following norm constraint:

$$\|K_i\|_2 < \sqrt{\zeta_i}\gamma_i. \tag{36}$$

Proof: To begin with, we denote $Y_i = P_i^{-1}, Z_i = K_i Y_i, \widehat{Q}_i = Y_i Q_i Y_i$. Since $Y_i P_i = \mathbb{I}_3$, (31) can be obtained directly. Subsequently, applying a congruence transformation to Π_i (9) with the block-diagonal matrix $\mathcal{Y}_i = \operatorname{diag}\{Y_i, \mathbb{I}_3\}$, we obtain the inequality $\Omega_i < 0$. Finally, to prevent $\|K_i\|_2$ from being so large that it adversely affects the performance of the onboard DCMGs for MEA, the following constraints are taken into account:

$$\|Z_i\|_2 < \sqrt{\zeta_i}, \tag{37}$$

and

$$\left\|Y_i^{-1}\right\|_2 < \gamma_i. \tag{38}$$

By applying the Schur complement to the above constraints (37) and (38), conditions (33) and (34) are derived. This completes the proof.

Remark 6: The LMIs (31)–(34) in Theorem 3 rely only on local parameters, independent of both power lines and other subsystems. The constrained parameters ζ_i in (33) and γ_i in (34) restrict the 2-norm of the controller gain to prevent excessive aggressiveness. Furthermore, the local controller is computed via the YALMIP interface in MATLAB, utilizing semidefinite programming solvers such as MOSEK and SDPT3.

Remark 7: The plugging in or out of a power source only causes the augmentation or reduction of a set of LMI conditions (31)–(34) and do not require updating

any existing controllers. This feature indicates that the proposed PnP voltage control method is scalable and ensures voltage stability. This approach adheres to privacy constraints, which is especially beneficial in energy markets where BESSs and RESs have distinct ownership [20], as depicted in Remark 2 and Table II.

The following Algorithm outlines the detailed procedure for designing the proposed PnP voltage controller in onboard DCMGs for MEA.

Algorithm 1 Design Procedure for the Proposed PnP Voltage Controller

Input: The onboard DCMG subsystem for MEA $\mathbb{M}_i$.
Output: The controller gain K_i.

1: Provide the electrical parameters of the local subsystem $\mathbb{M}_i$, thereby determining system matrices A_{ii}, B_i, H_i, and W_i. Additionally, specify the positive scalar $\hat{p}$, ϕ_i, and matrix G_i.
2: Define the decision variables in the LMI conditions from Theorem 3, including $\zeta_i, \gamma_i, Z_i, \widehat{Q}_i, S_i, R_i$, and Y_i. Subsequently, solve the LMI conditions to obtain the matrices Y_i and Z_i.
3: If the previous step yields a feasible solution, compute the controller gain K_i using $K_i = Z_i Y_i^{-1}$.

IV. SCALABLE PNP OPERATIONS

This section elaborates on the scalable plugging-in and unplugging operations under the proposed PnP control scheme.

Seamless plugging-in operation: Consider an interconnected dissipative onboard DCMG for MEA $\mathbf{M}_n$ equipped with PnP voltage controllers $\boldsymbol{K} = \text{diag}\{K_1, K_2, \ldots, K_n\}$, where the gain K_i is designed using Algorithm 1. When a new system $\mathbb{M}_{n+1}$ is integrated into the current system $\mathbf{M}_n$, the resulting system, denoted as $\mathbf{M}_{n+1} \doteq \mathbf{M}_n | \mathbb{M}_{n+1}$, retains dissipativity provided that the local controller K_{n+1} is derived through Algorithm 1. This ensures seamless integration without disrupting the dissipative properties of the network.

Smooth plugging-out operation: The disconnection of a subsystem is straightforward, as it does not require any modifications to the controllers. For an interconnected dissipative system $\mathbf{M}_n$ governed by PnP voltage controllers $\boldsymbol{K}$, the direct removal of an existing subsystem results in the reduced system $\mathbf{M}_{n-1} \doteq \mathbf{M}_n | \mathbb{M}_{n-1}$. The dissipativity of $\mathbf{M}_{n-1}$ is preserved, as each local controller $K_i,\ i \in \{1, 2, \ldots, n-1\}$ relies solely on its corresponding subsystem model, thereby ensuring stability without requiring additional modifications.

V. SIMULATION RESULTS

This section validates the efficacy of the proposed method through realistic computer simulations performed utilizing the Simulink's Specialized Power Systems toolbox. The topology of the simulated onboard DCMG for MEA, comprising six subsystems, is illustrated in Fig. 2. For each subsystem, the source voltages are set to $U_{si} = 400$ V. The power converters utilize non-ideal IGBT switches with a switching frequency of 15 kHz. The RLC filters and CPLs parameters are listed in columns 2 to 5 of Table III. As indicated in column 6 of Table III, the voltage reference values $U_{\text{ref}i}$ are slightly adjusted to induce power line currents I_{ij}, as shown in Fig. 1, in the steady-state regime. The parameters $\hat{p} = 10$, $\phi_i = 0.5$, and the matrix $G_i = [0.02, 0.02, 0.02]$ are utilized. Based on these parameters, the controller gains K_i, as derived in Theorem 3, are computed and presented in the last column of Table III.

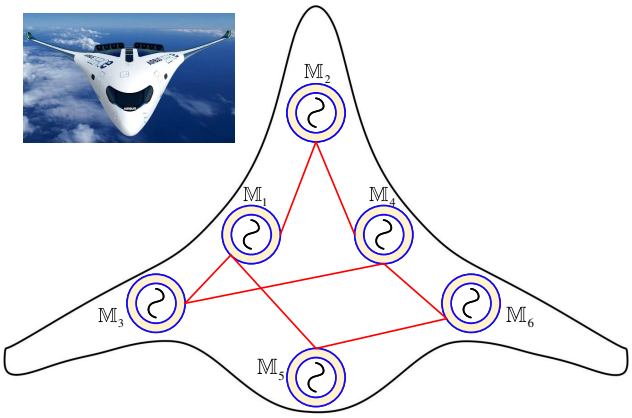

Fig. 2. Topology structure of the simulated MEA DCmGs.

A. Scenario 1: Scalable Voltage Stability Under Plugging-in/-out Operations

This scenario evaluates the scalable performance of the proposed PnP voltage control strategy during addition and removal operations of subsystems.

Initially, all power sources in the onboard DCMG for MEA are initialized but remain disconnected, with no energy exchange occurring among them. The proposed scalable voltage controllers u_i are activated to supply their respective CPLs and regulate the PCC voltages to their reference values $U_{\text{ref}i}$. At $t = 0.5$ s, power sources 1–5 are connected to establish a MEA system $\mathbf{M}_5$, whereas power source 6 remains disconnected at this time. At $t = 1$ s, subsystem $\mathbb{M}_6$ is integrated, and at $t = 1.5$ s, $\mathbb{M}_5$ is disconnected from the system $\mathbf{M}_5$.

As depicted in Fig. 3(a), during the interval from 0 to 0.5 s, subsystems 1–6 operate independently as isolated islands, supplying their respective CPLs. The voltage responses exhibit minor fluctuations from their desired reference values $U_{\text{ref}i}$ during initialization, integration, and disconnection processes, and quickly recover to their desired values. Fig. 3(b) illustrates the control input u_i, represented by the duty cycles of the power converters. These results indicate that the proposed control approach successfully regulates the PCC voltages with minimal error and short transient periods, highlighting its scalability for PnP operations.

TABLE III

Simulated parameters and controller gains for subsystem $\mathbb{M}_i,\ i = \{1, \ldots, 6\}$

$\mathbb{M}_i$	$R_{\mathrm{f}}(\Omega)$	L_{f}(mH)	C_{f}(mF)	P_{ℓ}(W)	U_{ref}(V)	Partial failure	Bias failure	Local controller gain K_i
1	0.2	1.8	2.2	100	250	5%	20	$[-0.413 \quad -0.211 \quad 65.149]$
2	0.3	2.0	1.9	120	240	10%	22	$[-0.398 \quad -0.187 \quad 63.152]$
3	0.1	2.2	1.7	105	230	15%	24	$[-2.310 \quad -0.593 \quad 81.773]$
4	0.5	3.0	2.5	95	220	14%	26	$[-0.513 \quad -0.295 \quad 99.169]$
5	0.4	1.2	2.0	110	210	15%	28	$[-0.166 \quad -0.292 \quad 81.017]$
6	0.6	2.5	3.0	105	200	20%	30	$[-2.701 \quad -0.188 \quad 87.247]$

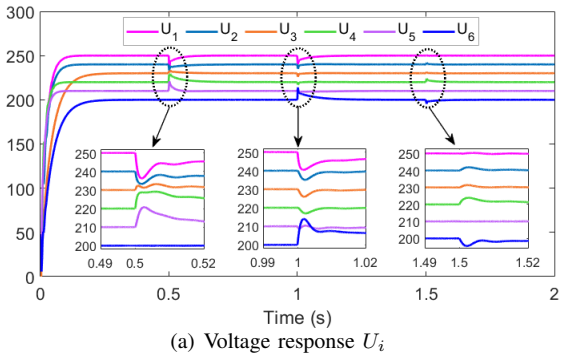

(a) Voltage response U_i

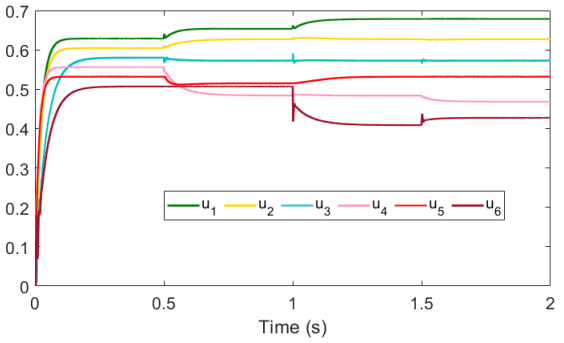

(b) Control input u_i

Fig. 3. Scalability of the proposed control scheme to PnP operations, illustrating the initialization of $\mathbb{M}_i$ 1–5 at $t = 0.5$ s, the integration of $\mathbb{M}_6$ at $t = 1.0$ s, and the disconnection of $\mathbb{M}_5$ at $t = 1.5$ s.

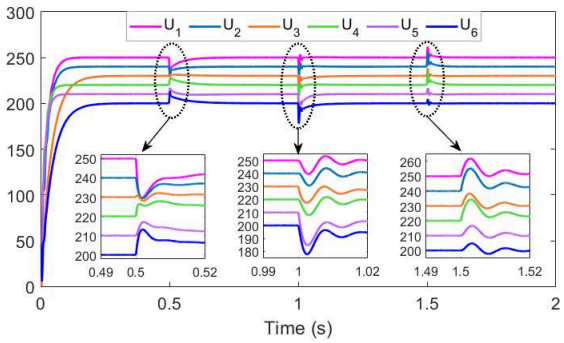

(a) Voltage response U_i

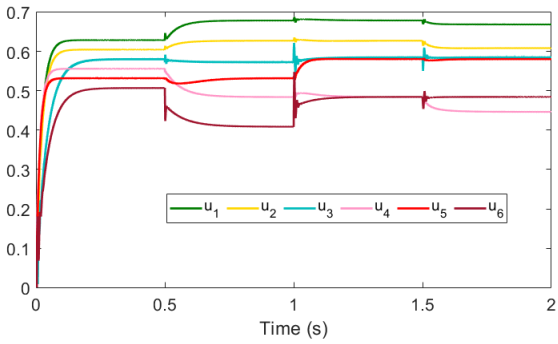

(b) Control input u_i

Fig. 4. Robustness of the proposed control scheme to varying CPLs, illustrating the initialization of $\mathbb{M}_i$ 1–6 at $t = 0.5$ s, the increase in power demands at $t = 1.0$ s, and the decrease at $t = 1.5$ s.

Notably, at $t = 0.5$ s, the voltage response of $\mathbb{M}_6$ remains unchanged as it has not yet been integrated into the system, yet it maintains autonomous islanding capability. Similarly, a non-zero constant voltage is maintained when $\mathbb{M}_5$ is disconnected at $t = 1.5$ s.

B. Scenario 2: Robust Voltage Stability Under Varying Power Demands of CPLs

This case examines the controller's robustness to dynamic variations in CPL power demands. In practical MEA scenarios, CPL power demands fluctuate significantly due to operational and environmental factors. For instance, flight control systems and avionics experience increased power demands during takeoff and landing, while reduced demands occur during cruising. Environmental factors, such as temperature variations, also influence the power consumption of thermal management systems. These variations necessitate a robust control strategy to maintain voltage stability under dynamic load conditions.

At $t = 0$ s, all subsystems are initially disconnected and subsequently interconnected to form the MEA system $\mathbf{M}_6$ at $t = 0.5$ s. At $t = 1$ s, the CPL power demands increase as follows: $P_{\ell 3}$ rises to 135, $P_{\ell 5}$ to 158, and $P_{\ell 6}$ to 155, from the initial values listed in Table II. At $t = 1.5$ s, the power demands decrease as follows: $P_{\ell 1}$ drops to 80, $P_{\ell 2}$ to 95, and $P_{\ell 4}$ to 65. The proposed controller governs the entire process from start to finish.

As shown in Fig. 4(a), the voltage responses do not significantly deviate from their reference values, and the deviations disappear quickly after each change in power demand. The control inputs are depicted in Fig. 4(b). These results confirm that the proposed control approach robustly maintains voltage stability under varying CPL power demands.

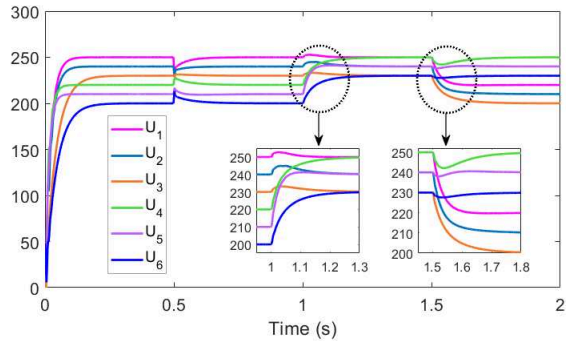

(a) Voltage response U_i

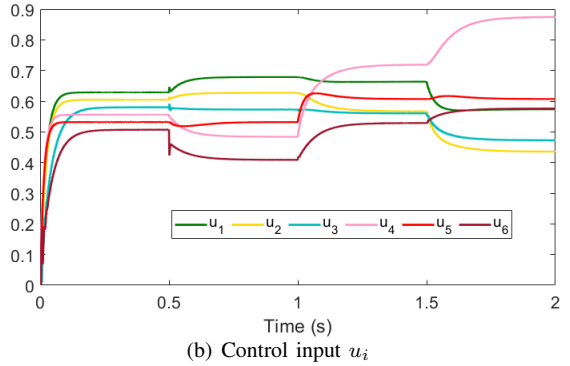

(b) Control input u_i

Fig. 5. Robustness of the proposed control scheme to varying voltage references, illustrating the initialization of $\mathbb{M}_i$ 1–6 at $t = 0.5$ s, the increase in voltage references at $t = 1.0$ s, and the decrease at $t = 1.5$ s.

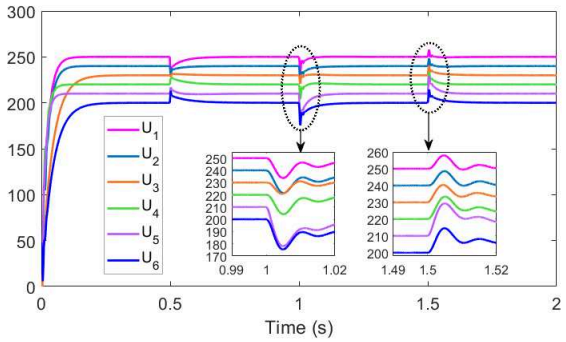

(a) Voltage response U_i

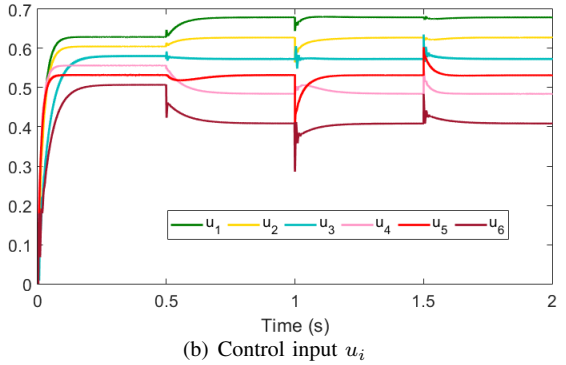

(b) Control input u_i

Fig. 6. Reliability of the proposed control scheme to actuator failures, illustrating the initialization of $\mathbb{M}_i$ 1–6 at $t = 0.5$ s, the occurrence of partial failures at $t = 1.0$ s, and the introduction of biases at $t = 1.5$ s.

C. Scenario 3: Robust Voltage Stability Under Fluctuating Voltage References

This case investigates the control strategy's ability to maintain stability under fluctuating voltage references $U_{\text{ref}i}$. In the MEA, voltage references may vary due to Energy Management System (EMS) adjustments or external factors. For example, EMS may raise voltage references during high-power phases (e.g., takeoff or emergencies) to ensure critical system performance, and lower them during low-power phases (e.g., cruising) to improve efficiency. External factors, such as temperature variations, may also necessitate reference adjustments to maintain optimal operation.

At $t = 0$ s, all subsystems are initially disconnected and then interconnected to build $\mathbf{M}_6$ at $t = 0.5$ s. At $t = 1$ s, the voltage reference values are adjusted as follows: $U_{\text{ref}4}$ increases to 250, $U_{\text{ref}5}$ to 240, and $U_{\text{ref}6}$ increases to 230. At $t = 1.5$ s, $U_{\text{ref}1}$ decreases to 220, $U_{\text{ref}2}$ to 210, and $U_{\text{ref}3}$ to 200.

As illustrated in Fig. 5(a), the voltage responses exhibit minimal deviations from their reference values during the adjustment process, with rapid recovery to the new set-points. The control inputs, shown in Fig. 5(b), can ensure such voltage stability. These results confirm that the proposed control strategy effectively maintains voltage stability despite fluctuating references, thereby demonstrating its robustness.

D. Scenario 4: Reliable Voltage Stability Subject to Actuator Failures

In practice, power electronic components in BESSs and RESs may experience reduced efficiency over time, leading to partial loss of control input effectiveness. Similarly, hardware degradation, environmental stress, or electromagnetic interference can introduce input biases, further compromising system performance [19]. These faults, if unaddressed, can destabilize the DCmGs and jeopardize the safe operation of critical aircraft systems.

In order to assess the reliability of the proposed method, we first form the MEA system $\mathbf{M}_6$ at $t = 0.5$ s, then simulate scenarios where control inputs experience partial loss of effectiveness at $t = 1$ s and an input bias is introduced at $t = 1.5$ s. The values for these failures are provided in columns 7 and 8 of Table III.

As shown in Fig. 6(a), the voltage responses remain close to their reference values, with only minor deviations that quickly disappear. The corresponding control inputs, depicted in Fig. 6(b), demonstrate the controller's fault-tolerant capability in mitigating actuator failures. These results confirm that the proposed scheme enhances system reliability, ensuring stable operation even in the presence of actuator failures.

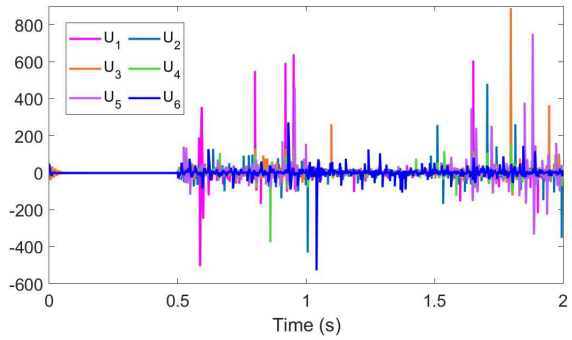

(a) Voltage tracking at PCCs without controllers.

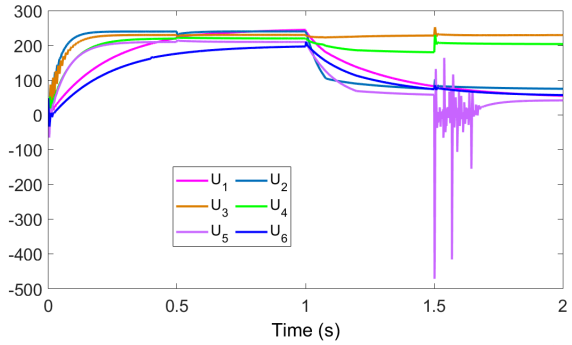

(b) Voltage tracking at PCCs using the control method in [25].

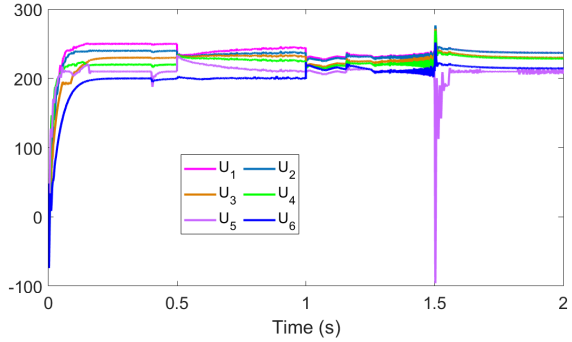

(c) Voltage tracking at PCCs using the control method in [20].

Fig. 7. Comparative analysis with three representative benchmark approaches under PnP operations.

E. Scenario 5: Comparative Analysis With Existing Methods

To further assess the effectiveness of the proposed PnP voltage control strategy, comparative simulations are performed against three representative benchmarks: 1) open-loop voltage response (i.e., without any controller), 2) a sliding mode control method for CPLs from [25] without PnP functionality, and 3) a PnP control approach from [20] that does not account for CPLs. The corresponding voltage responses are shown in Fig. 7(a)–(c).

As depicted in Fig. 7(a), the open-loop case exhibits pronounced voltage deviations and sustained oscillations throughout the operation. Such large fluctuations can impose considerable electrical and thermal stress on power semiconductor devices (e.g., IGBTs, MOSFETs), which have been reported by approximately 34% of manufacturers as among the most failure-prone components [19], thereby reducing system reliability. In Fig. 7(b), the sliding mode method in [25] achieves satisfactory voltage response during the initial stage, benefiting from its capability to handle CPLs. However, the absence of PnP adaptability leads to instability during subsystem integration at $t = 1$ s and disconnection at $t = 1.5$ s, with the voltages failing to return to their reference values and exhibiting noticeable oscillations. As shown in Fig. 7(c), the PnP control method from [20] maintains operation during plugging-in/out of subsystems but suffers from pronounced voltage fluctuations in the presence of CPLs. The inherent nonlinear and negative impedance characteristics of CPLs cause uneven voltage recovery during plug-in events and severe transients during disconnection.

In contrast, as depicted in Fig. 3(a), the proposed method achieves rapid convergence during plug-in operations, with a settling time of approximately 0.02 s and voltage fluctuations limited to within 10 V. During plug-out events, the convergence time is further reduced to around 0.1 s, with fluctuations contained within 5 V. These results confirm that the proposed controllers maintain stability and satisfy IEEE voltage regulation criteria [38] under dynamic PnP operations.

Overall, across all tested conditions, the proposed control strategy demonstrates superior dynamic response and voltage regulation accuracy compared with the benchmark approaches.

VI. CONCLUSION

This paper has proposed a PnP voltage control scheme of onboard DCMGs for MEA, enabling seamless connection and disconnection of BESSs/RESs in the presence of CPLs. By adopting the structured storage function method, the study ensures the dissipative voltage stability of both local and global systems, addressing scalability challenges associated with PnP operations of various power sources. Moreover, the proposed approach robustly handles parameter variations in CPL power and reference voltage, while ensuring reliable operation during fault events. The effectiveness of the proposed strategy is validated through realistic simulations using the Specialized Power Systems toolbox of Simulink.

Future research will focus on developing PnP fault detection, diagnosis, and isolation techniques to promptly disconnect faulty subsystems or power grids, preventing fault propagation and escalation in MEA.

REFERENCES

[1] P. J. Ansell and K. S. Haran, "Electrified airplanes: A path to zeroemission air travel," *IEEE Electrific. Mag.*, vol. 8, no. 2, pp. 18–26, Jun. 2020.

[2] D. Wang, S. Hemming, Y. Yang, A. Poorfakhraei, L. Zhou, C. Liu, and A. Emadi, "Multilevel inverters for electric aircraft applications: Current status and future trends," *IEEE Trans. Ind. Electron.*, vol. 10, no. 2, pp. 3258–3282, Jun. 2024.

[3] C. -M. Liaw, P. -H. Jhou, and C. -W. Yang, "Switched-reluctance motor drive for more electric aircraft with energy storage buffer," *IEEE Trans. Aerosp. Electron. Syst.*, vol. 59, no. 6, pp. 7423–7439, Dec. 2023.

[4] B. Sarlioglu and C. T. Morris, "More electric aircraft: Review, challenges, and opportunities for commercial transport aircraft," *IEEE Trans. Transport. Electrific.*, vol. 1, no. 1, pp. 54–64, Jun. 2015.

[5] R. P. Venturini, P. Mattavelli, P. Zanchetta, and M. Sumner, "Adaptive selective compensation for variable frequency active power filters in more electrical aircraft," *IEEE Trans. Aerosp. Electron. Syst.*, vol. 48, no. 2, pp. 1319–1328, Apr. 2012.

[6] G. Buticchi, S. Bozhko, M. Liserre, P. Wheeler, and K. Al-Haddad, "On-board microgrids for the more electric aircraft–Technology review," *IEEE Trans. Ind. Electron.*, vol. 66, no. 7, pp. 5588–5599, Jul. 2019.

[7] L. Ding, Q. -L. Han, L. Y. Wang, and E. Sindi, "Distributed cooperative optimal control of DC microgrids with communication delays," *IEEE Trans. Ind. Inform.*, vol. 14, no. 9, pp. 3924–3935, Sep. 2018.

[8] J. Su and K. Li, "Differential power processing based control framework for multiple battery energy storage systems in DC microgrids," *IEEE Trans. Sustain. Energy*, vol. 15, no. 4, pp. 2417–2427, Oct. 2024.

[9] A. Barzkar and M. Ghassemi, "Components of electrical power systems in more and all-electric aircraft: A review," *IEEE Trans. Transport. Electrific.*, vol. 8, no. 4, pp. 4037–4053, Dec. 2022.

[10] A. -C. Braitor, H. Siguerdidjane, and A. Iovine, "On the voltage stability and network scalability of onboard DC microgrids for hybrid electric aircraft," *IEEE Trans. Aerosp. Electron. Syst.*, vol. 60, no. 4, pp. 5350–5358, Aug. 2024.

[11] Y. Zhang, G. O. H. Peng, J. K. Banda, S. Dasgupta, M. Husband, R. Su, and C. Y. Wen, "An energy efficient power management solution for a fault-tolerant more electric engine/aircraft," *IEEE Trans. Ind. Electron.*, vol. 66, no. 7, pp. 5663–5675, Jul. 2019.

[12] R. Rohrmueller and B. Annighoefer, "Hypervisors and plug & fly in a new space launcher: A scalable approach to enhance space launcher development," *2024 AIAA DATC/IEEE 43rd Digital Avionics Systems Conference (DASC)*, San Diego, CA, USA, 2024, pp. 1–9.

[13] A. Wang, M. Fei, Y. Song, D. Du, C. Peng, and K. Li, "Scalable fuzzy control for nonlinear DC microgrids under plug-and-play operations," *IEEE Trans. Fuzzy Syst.*, vol. 32, no. 8, pp. 4747–4758, Aug. 2024.

[14] J. Xu, X. Chen, Y. Tan, and K. Zhou, "Multi-objective complementary control," *IEEE Trans. Autom. Control*, vol. 70, no. 6, pp. 3556–3570, Jun. 2025.

[15] I. Kouveliotis-Lysikatos, D. I. Koukoula, A. L. Dimeas, and N. D. Hatziargyriou, "Plug-and-play algorithms for the efficient coordination of active distribution grids," *Proc. IEEE*, vol. 110, no. 12, pp. 1927–1939, Dec. 2022.

[16] S. Günter, G. Buticchi, G. D. Carne, C. Gu, M. Liserre, H. Zhang, and C. Gerada, "Load control for the DC electrical power distribution system of the more electric aircraft," *IEEE Trans. Power Electron.*, vol. 34, no. 4, pp. 3937–3947, Apr. 2019.

[17] A. Griffo and J. Wang, "Large signal stability analysis of 'More Electric' aircraft power systems with constant power loads," *IEEE Trans. Aerosp. Electron. Syst.*, vol. 48, no. 1, pp. 477–489, Jan. 2012.

[18] L. Xing, Z. Shu, J. Fang, C. Wen, and C. Zhang, "Distributed control of DC microgrids: A relaxed upper bound for constant power loads," *Automatica*, vol. 173, Mar. 2025, Art. no. 112021.

[19] A. Wang, M. Fei, and Y. Song, "A novel scalable and reliable control for DC microgrids with varying number of agents," *IEEE Trans. Cybern.*, vol. 54, no. 9, pp. 4962–4972, Sep. 2024.

[20] M. Tucci, S. Riverso, and G. Ferrari-Trecate, "Line-independent plug-and-play controllers for voltage stabilization in DC microgrids," *IEEE Trans. Control Syst. Technol.*, vol. 26, no. 3, pp. 1115–1123, May 2018.

[21] A. Wang, M. Fei, D. Du, C. Peng, and K. Li, "Scalable neural network control for nonlinear DC microgrids under plug-and-play operations," *IEEE Trans. Ind. Inform.*, vol. 21, no. 5, pp. 3849–3859, May 2025.

[22] A. V. P. Premakumar, Y. -Y. Qian, M. Davoodi, Y. Wan, and A. Davoudi, "Robust control of power buffers in DC microgrids," *IEEE Trans. Energy Convers.*, vol. 38, no. 1, pp. 89–99, Mar. 2023.

[23] M. S. Sadabadi, Q. Shafiee, and A. Karimi, "Plug-and-play robust voltage control of DC microgrids," *IEEE Trans. Smart Grid*, vol. 9, no. 6, pp. 6886–6896, Nov. 2018.

[24] J. Su, K. Li, and C. Xing, "Plug-and-play of grid-forming units in DC microgrids assisted with power buffers," *IEEE Trans. Smart Grid*, vol. 15, no. 2, pp. 1213–1226, Mar. 2024.

[25] Z. Zuo, N. Vafamand, S. Mobayen, and T. Dragičević, "Finite-time tracking control with fast reaching condition for disturbed more electric aircraft direct current microgrid with constant power loads," *IEEE Trans. Aerosp. Electron. Syst.*, vol. 59, no. 5, pp. 6695–6704, Oct. 2023.

[26] M. A. A. Mohamed, M. Rashed, X. Lang, J. Atkin, S. Yeoh, and S. Bozhko, "Droop control design to minimize losses in dc microgrid for more electric aircraft," *Elect. Power Syst. Res.*, vol. 199, Oct. 2021, Art. no. 107452.

[27] F. Gao, S. Bozhko, G. Asher, P. Wheeler, and C. Patel, "An improved voltage compensation approach in a droop-controlled dc power system for the more electric aircraft," *IEEE Trans. Power Electron.*, vol. 31, no. 10, pp. 7369–7383, Oct. 2016.

[28] P. Magne, B. Nahid-Mobarakeh, and S. Pierfederici, "Active stabilization of DC microgrids without remote sensors for more electric aircraft," *IEEE Trans. Ind. Appl.*, vol. 49, no. 5, pp. 2352–2360, Sep./Oct. 2013.

[29] D. Zhao, K. Shen, L. Chen, Z. Wang, W. Liu, T. Yang, and P. Wheeler, "Improved active damping stabilization of DAB converter interfaced aircraft dc microgrids using neural network-based model predictive control," *IEEE Trans. Transp. Electrific.*, vol. 8, no. 2, pp. 1541–1552, Jun. 2022.

[30] S. Yousefizadeh, J. D. Bendtsen, N. Vafamand, M. H. Khooban, F. Blaabjerg, and T. Dragičević, "Tracking control for a DC microgrid feeding uncertain loads in more electric aircraft: Adaptive backstepping approach," *IEEE Trans. Ind. Electron.*, vol. 66, no. 7, pp. 5644–5652, Jul. 2019.

[31] F. Dörfler and F. Bullo, "Kron reduction of graphs with applications to electrical networks," *IEEE Trans. Circuits Syst. I–Regul. Pap.*, vol. 60, no. 1, pp. 150–163, Jan. 2013.

[32] V. Venkatasubramanian, H. Schattler, and J. Zaborszky, "Fast time-varying phasor analysis in the balanced three-phase large electric power system," *IEEE Trans. Autom. Control*, vol. 40, no. 11, pp. 1975–1982, Nov. 1995.

[33] T. Dragičević, X. Lu, J. C. Vasquez, and J. M. Guerrero, "DC microgrids–Part II: A review of power architectures, applications, and standardization issues," *IEEE Trans. Power Electron.*, vol. 31, no. 5, pp. 3528–3549, May 2016.

[34] D. Ye, J. H. Park, and Q. Y. Fan, "Adaptive robust actuator fault compensation for linear systems using a novel fault estimation mechanism," *Int. J. Robust Nonlinear Control*, vol. 26, no. 8, pp. 1597–1614, May 2016.

[35] S. Hu, P. Yuan, D. Yue, C. Dou, Z. Cheng, and Y. Zhang, "Attack-resilient event-triggered controller design of DC microgrids under DoS attacks," *IEEE Trans. Circuits Syst. I–Regul. Pap.*, vol. 67, no. 2, pp. 699–710, Feb. 2020.

[36] R. Merris, "Laplacian matrices of graphs: A survey," *Linear Alg. Appl.*, vol. 197–198, pp. 143–176, Jan.–Feb. 1994.

[37] N. Kottenstette, M. J. McCourt, M. Xia, V. Gupta, and P. J. Antsaklis, "On relationships among passivity, positive realness, and dissipativity in linear systems," *Automatica*, vol. 50, no. 4, pp. 1003–1016, Apr. 2014.

[38] *IEEE Recommended Practice for Monitoring Electric Power Quality,* IEEE Standard 1159, 2009.

Aimin Wang (Graduate Student Member, IEEE) received the M.Eng. degree in control engineering from Hangzhou Dianzi University, Hangzhou, China, in 2021. He is currently pursuing the Ph. D. degree in control science and engineering at Shanghai University, Shanghai, China. From 2024 to 2025, he was a visiting Ph. D. student with the College of Design and Engineering at National University of Singapore, Singapore. His current research interests include scalable control, plug-and-play control, and fault-tolerant control for renewable energy systems.

Minrui Fei received his B.S. and M.S. degrees in Industrial Automation from the Shanghai University of Technology in 1984 and 1992, respectively, and his PhD degree in Control Theory and Control Engineering from Shanghai University in 1997. Since 1998, he has been a full professor at Shanghai University. He is Chairman of Embedded Instrument and System Sub-society, and Fellow and Director of China Instrument & Control Society; Honorary Vice-president and Fellow of China Simulation Federation, Vice-chairman of Intelligent Control and Intelligent Management Sub-society, Fellow of AsiaSim and China Simulation Federation. His research interests are in the areas of networked control systems, intelligent control, complex system modeling, hybrid network systems, and field control systems.

Xue Li (Member, IEEE) received the B.Sc. degree in electrical technology, and M.Sc. degree in power system and automation from Zhengzhou University, Zhengzhou, China, in 2002 and 2006, respectively, and the Ph. D. degree in control theory and control engineering from Shanghai University, Shanghai, China, in 2009. She is currently a Professor in Shanghai University. Her main research interests include security control and performance assessment of smart grids.

Chen Peng (Senior Member, IEEE) received the M.Sc. and Ph.D. degrees from the Chinese University of Mining Technology, Xuzhou, China, in 1999 and 2002, respectively. From September 2002 to August 2004, he was a Postdoctoral Research Fellow in applied math with Nanjing Normal University, Nanjing, China. From November 2004 to January 2005, he was a Research Associate with Hong Kong University, Hong Kong. From July 2006 to August 2007, he was a Visiting Scholar with the Queensland University of Technology, Brisbane, Australia. From September 2010 to August 2012, he was a Postdoctoral Research Fellow with Central Queensland University, Rockhampton, Australia. He is currently a Professor with the School of Mechatronic Engineering and Automation, Shanghai University, Shanghai, China. His current research interests include networked control systems, multi-agent systems, power systems, and interconnected systems. Prof. Peng is an Associate Editor of a number of international journals, including the IEEE TRANSACTIONS ON INDUSTRIAL INFORMATICS, Information Sciences, and Transactions of the Institute of Measurement and Control. He was named a Highly Cited Researcher from 2020 to 2022 by Clarivate Analytics.

Kang Li (Senior Member, IEEE) received the B.Sc. degree in industrial automation from Xiangtan University, Hunan, China, in 1989, the M.Sc. degree in control theory and applications from Harbin Institute of Technology, Harbin, China, in 1992, the Ph.D. degree in control theory and applications from Shanghai Jiaotong University, Shanghai, China, in 1995, and the D.Sc. degree in engineering from Queen's University Belfast, Belfast, U.K., in 2015., From 1995 to 2002, he was a Research Fellow with Shanghai Jiaotong University, Delft University of Technology, and Queen's University Belfast. From 2002 to 2018, he was with the School of Electronics, Electrical Engineering and Computer Science, Queen's University Belfast, where he was a Lecturer, in 2002, a Senior Lecturer, in 2007, a Reader, in 2009, and a Chair Professor, in 2011. He currently holds the Chair of Smart Energy Systems with the University of Leeds, Leeds, U.K. His research interests include nonlinear system modeling, identification, and control, and artificial intelligence, with applications to energy and power systems, smart grids, electric vehicles, electrification of railway systems, and energy management in energy-intensive manufacturing processes.

Chi Yung Chung (Fellow, IEEE) received the B.Eng. (Hons.) and Ph.D. degrees in electrical engineering from The Hong Kong Polytechnic University, Hong Kong, China, in 1995 and 1999, respectively.

He is currently the Head of the Department of Electrical and Electronic Engineering, the Chair Professor of Power Systems Engineering, and the Founder and the Director of the Research Centre for Grid Modernisation, The Hong Kong Polytechnic University. His research interests include smart grid technologies, renewable energy, power system stability/control, planning and operation, computational intelligence applications, power markets, and electric vehicle charging.

Dr. Chung is the President-Elect of the IEEE PES, a Fellow of CAE, EIC, CSEE, IET, and HKIE, and the IEEE PES Distinguished Lecturer. He was a recipient of the 2021 IEEE Canada P. Ziogas Electric Power Award. He has been a Senior Editor of IEEE TRANSACTIONS ON POWER SYSTEMS, a Consulting Editor of IEEE TRANSACTIONS ON SUSTAINABLE ENERGY, and the Vice Editor-in-Chief of JOURNAL OF MODERN POWER SYSTEMS AND CLEAN ENERGY.